The Gaussian Curvature Elastic Energy of Intermediates in Membrane Fusion

David P. Siegel
Givaudan, Inc., Cincinnati, Ohio

ABSTRACT The Gaussian curvature elastic energy contribution to the energy of membrane fusion intermediates has usually been neglected because the Gaussian curvature elastic modulus, κ, was unknown. It is now possible to measure κ for phospholipids that form bicontinuous inverted cubic (Q_{II}) phases. Here, it is shown that one can estimate κ for lipids that do not form Q_{II} phases by studying the phase behavior of lipid mixtures. The method is used to estimate κ for several lipid compositions in excess water. The values of κ are used to compute the curvature elastic energies of stalks and catenoidal fusion pores according to recent models. The Gaussian curvature elastic contribution is positive and similar in magnitude to the bending energy contribution: it increases the total curvature energy of all the fusion intermediates by 100 units of k_BT or more. It is important to note that this contribution makes the predicted intermediate energies compatible with observed lipid phase behavior in excess water. An order-of-magnitude fusion rate equation is used to estimate whether the predicted stalk energies are consistent with the observed rates of stalk-mediated processes in pure lipid systems. The current theory predicts a stalk energy that is slightly too large, by $\sim$30 k_BT, to rationalize the observed rates of stalk-mediated processes in phosphatidylethanolamine or *N*-monomethylated dioleoylphosphatidylethanolamine systems. Despite this discrepancy, the results show that models of fusion intermediate energy are accurate enough to make semiquantitative predictions about how proteins mediate biomembrane fusion. The same rate model shows that for proteins to drive biomembrane fusion at observed rates, they have to perform mediating functions corresponding to a reduction in the energy of a purely lipidic stalk by several tens of k_BT. By binding particular peptide sequences to the monolayer surface, proteins could lower fusion intermediate energies by altering the elastic constants of the patches of lipid monolayer that form the stalk. Here, it is shown that if peptide binding changes κ or some other combinations of local elastic constants by only tens of percents, the stalk energy and the energy of catenoidal fusion pores would decrease by tens of k_BT relative to the pure lipid value. This is comparable to the required mediating effect. The curvature energies of stalks and catenoidal fusion pores have almost the same dependence on monolayer elastic constants as the curvature energies of the rhombohedral and Q_{II} phases; respectively. The effects of isolated fusion-relevant peptides on the energies of these intermediates can be determined by studying the effects of the peptides on the stability of rhombohedral and Q_{II} phases.

INTRODUCTION

The structures of intermediates in the process of biomembrane fusion are difficult to establish, since the intermediates are small and transient. However, using information obtained from the study of model lipid systems, it is possible to estimate the energy of different proposed intermediate structures relative to the initial flat bilayer state. This energy is taken to represent the minimum activation energy for membrane fusion. It is thus possible to postulate mechanisms for membrane fusion by looking for mechanisms in which the intermediate structures have low free energy and change with lipid composition in a fashion compatible with the observed composition-dependent membrane fusion rates. To date, no fusion mechanism has been proposed that proceeds via lower-energy structures than the recent versions of the stalk mechanism (1–4). In particular, the mechanism described by Kozlovsky and colleagues (2,3) has been successful in rationalizing many qualitative observations concerning the lipid composition dependence of membrane fusion rates (5–7), and seems compatible with many observations of protein-mediated biomembrane fusion (6–9).

The principal components of the energies of a fusion intermediate like a stalk are the energy necessary to closely oppose the surfaces of the two original bilayers (10,11); the curvature elastic energies of the lipid monolayers; and the energy associated with stabilization of hydrophobic defects (1,12). The latter contribution arises through local variations in lipid acyl chain length or in lipid molecule tilt (2). The curvature energies of intermediates in fusion can be calculated using the Helfrich expression for the lipid monolayer curvature energy (13). The Helfrich curvature energy is composed of contributions from the bending energy and the Gaussian curvature elastic energy.

Most authors have either neglected the contribution of the Gaussian curvature elastic energy in calculating the curvature energy of fusion intermediates (1–4,12), or have assumed that the contribution is very small (14). An awkward feature of some of these theories is that their predictions contradict observed lipid phase behavior. Some predict the existence of lipid phases not previously observed for some ranges of lipid

Submitted June 16, 2008, and accepted for publication September 3, 2008.

Address reprint requests to David P. Siegel, Givaudan, Inc., 1199 Edison Dr., Cincinnati, OH 45216. Tel: 513-948-4840; E-mail: david.siegel@givaudan.com.

Editor: Peter Tieleman.

0006-3495/08/12/5200/16 $2.00

doi: 10.1529/biophysj.108.140152

spontaneous curvature, such as phases composed of stalks for sufficiently negative values of the spontaneous curvature (1,2), or inverted cubic phases for any lipid with negative spontaneous curvature above the chain-melting temperature (14), where only lamellar phases are observed. The theory of May (4) deals only with stalks. It predicts stalk energies that are >0 for values of spontaneous curvature $>\sim -0.35\ \mathrm{nm}^{-1}$, and hence is compatible with the observed absence of stable stalk phases in pure PE and lipids with more positive curvatures in excess water.

One of the reasons for calculating the energy of fusion intermediates is to help us understand how proteins mediate membrane fusion in vivo. For our models to be useful for this purpose, the predictions must be compatible with two sets of observations on pure lipid systems. First, they must be compatible with observed lipid phase behavior. If they do not pass this test, then they are incorrectly predicting the curvature energy of monolayer assemblies. Second, the predicted fusion intermediate energies must be compatible with the observed rates of lipid mixing and fusion in pure lipid systems. It is therefore important to calculate the energies of fusion intermediates containing the Gaussian curvature energy contribution, and determine whether the results are consistent with these observations.

A recent theoretical study (11) showed that inclusion of the Gaussian curvature contribution is necessary to rationalize the lipid composition and water activity ranges of stability of the rhombohedral phase, in which the structural unit is essentially a stalk fusion intermediate. In Kozlovsky et al. (11), the contribution of the Gaussian curvature elastic energy to the stalk energy is positive and comparable to that of the bending in absolute magnitude. These results imply that the Gaussian curvature elastic energy is a substantial component of the curvature energy of fusion intermediates, and that neglecting it produces substantial under-estimates of intermediate energies relative to planar bilayers.

To calculate the Gaussian curvature contribution to the curvature energy, the Gaussian curvature elastic modulus must be known (13), and this modulus is lipid composition-dependent (15,16). Recently, accurate methods for measuring the Gaussian curvature modulus have been developed (17–19), although they have so far been applied to only two lipid compositions. One factor limiting wider application of these methods is that they can only be used on lipid compositions that adopt bicontinuous inverted cubic (Q_{II}) phases. Here, the method employed by Siegel (19) is extended to estimate the Gaussian curvature elastic moduli of additional lipid compositions that are more representative of biomembrane lipids. Observations of lipid phase behavior from earlier x-ray diffraction and ^{31}P NMR studies, along with data previously obtained with *N*-monomethylated dioleoylphosphatidylethanolamine (DOPE-Me (20)), are used to estimate the moduli for DOPE, dioleoylphosphatidylcholine (DOPC), and an equimolar mixture of DOPC and cholesterol.

The derived values of the Gaussian curvature moduli results are then used to calculate the curvature energy for stalks and catenoidal fusion pores for several lipid compositions using recently derived models (11,18). It is shown that the Gaussian curvature elastic energy contribution is positive and of the same order of magnitude as the bending energy contribution for stalks, hemifusion diaphragms, and catenoidal fusion pores in all of the lipid compositions. The Gaussian curvature elastic contribution makes the total curvature energy of the fusion intermediates larger than values obtained using only the bending energy by 100–200 units of k_BT, where k_B is the Boltzmann constant and T is the temperature. The resulting intermediate energies are compatible with the observed phase behavior of these lipids in excess water. An order-of-magnitude estimate of stalk formation rates in pure lipid systems is used to determine whether the curvature energies of stalks, including the Gaussian curvature elastic energy contributions, are consistent with the observed rates of stalk-mediated processes in pure lipid systems. We presume that membrane fusion-mediating proteins act in part by reducing the energy necessary to create fusion intermediates. To estimate the extent of this reduction, we use the same model of stalk formation rates that would be required for stalks to form on the observed timescale of membrane fusion in two representative biomembrane systems.

THEORY

Fig. 1 is a schematic diagram of the stalk-mediated fusion of two unilamellar bilayer liposomes (5,6). The monolayers of the bilayers are depicted as continuous slabs. The two original liposomes interact through formation of a stalk between the proximal monolayers (Fig. 1 *A*), which, at the narrowest point in a plane parallel to the original bilayers, has a radius equal to that of one lipid monolayer thickness. The stalk expands in the plane of the bilayers into a hemifusion diaphragm (HF) (Fig. 1 *B*), which corresponds to a stalk with a disk of planar bilayer inserted in the center. According to a recent model (3), radial expansion of the stalk is spontaneous for lipids with negative values of spontaneous curvature (J_s), like DOPE, but requires an applied membrane tension for lipids with larger (less negative) values, like DOPC. The planar bilayer in the center of the HF can form a fusion pore (Fig. 1 *C*) within the single bilayer diaphragm. It is not clear what the shape of the fusion pore is or where it will form in the HF, although it likely forms at the edge of the diaphragm (3). The pore in the HF is unstable due to the high curvature energy of the pore edges ($\sim 3\ k_BT$/nm of edge length (6)). We presume that the system rearranges by a combination of radial contraction of the rim of the HF and radial expansion of the fusion pore in the planar bilayer expansion to form a more stable bilayer-walled pore (Fig. 1 *D*). Here, the bilayer-walled pore is referred to as the catenoidal fusion pore. This is because when the two monolayers have the same composition, the minimal-curvature energy form of this pore is achieved when the bilayer midplanes lie on a catenoid (18), which is a zero-curvature surface. The catenoidal fusion pore has also been referred to as an interlamellar attachment (18,19), although earlier uses of this term referred to bilayer-walled pores with a noncatenoidal shape(e.g., (12,14)). It has been proposed that the first fusion pore can also form directly from the stalk, as well as from the HF, based on the results of fluorescence assays in polyethylene glycol (PEG)-induced fusion (21) and coarse-grain computer simulations (22).

The HF-to-catenoidal pore rearrangement process must require a substantial input in energy in the form of applied tension in systems with low J_s, since radial contraction of the HF rim is not spontaneous (3). In fusion

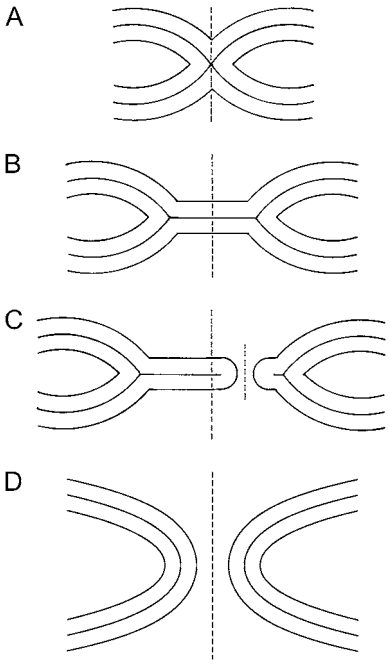

FIGURE 1 Schematic representation of fusion according to the stalk theory (2,3). The monolayers of the bilayers are depicted as slabs. All structures are axially symmetric and appear in the cross section that contains their vertical axes (*dotted lines*). The first structure to form that bridges two opposed membranes is the stalk (*A*). For sufficiently negative values of J_s (3), or in the presence of sufficient membrane tension, the stalk can expand radially to form a hemifusion diaphragm (*B*), which contains a disk of planar bilayer membrane in the center. Fusion occurs when a pore forms within this single bilayer (*C*). The axis of the pore is depicted as the shorter vertical dashed line. The edge of the bilayer pore is unstable, and the system can lower its free energy by forming a catenoidal fusion pore (*D*).

involving planar lipid bilayers made with alkane solvents (23), it is possible that residual solvent lowers the defect stabilization energy inherent to the HF rims (12), but this does not occur in phospholipid unilamellar vesicles made via extrusion (24). Catenoidal fusion pores form in 0.1- to 0.2-μm extruded unilamellar vesicles of DOPE-Me within milliseconds after they are temperature-jumped above the bilayer/nonbilayer phase transition temperature (24). Thus, it is possible that fusion pore formation can occur after limited expansion of the HF (Fig. 1 *C*) in protein-free, solvent-free membranes (12). In this work, due to the uncertainty in the structure and dimensions of the initial fusion pore, only the curvature energy of the catenoidal fusion pore (Fig. 1 *D*) will be calculated, because the geometry is more constrained.

The curvature elastic energy per unit area of a continuous monolayer with respect to a planar monolayer is given as (13)

$$f = \frac{k_m}{2}[J - J_s]^2 + \kappa K - \frac{k_m}{2}J_s^2, \qquad (1)$$

where J is the monolayer curvature at the monolayer neutral plane, J_s the spontaneous curvature at the same plane, k_m the monolayer bending modulus, and κ the monolayer Gaussian modulus. The curvature is represented by $J = c_1 + c_2$ and the Gaussian curvature by $K = c_1c_2$, where c_1 and c_2 are the two principal radii of curvature of the monolayer neutral plane. The sign of κ for lipid monolayers is negative to be consistent with observed lipid phase behavior. In bicontinuous Q_{II} phases, c_1 and c_2 are of different sign, and $K < 0$. If κ is ≥ 0, it can be shown that Q_{II} phases form instead of lamellar phases for all lipids with even slightly negative values of J_s (18), like DOPC, and the Q_{II} phases immediately collapse to very small values of the unit cell constant to maximize the area density of K.

Models for stalk structure composed of smooth monolayers predict high curvature energies for stalks (12,14) because of the attendant creation of hydrophobic interstices at the juncture where the hydrophobic surfaces of the monolayers separate. These interstices must be stabilized by entropically disfavored stretching of the surrounding acyl chains, which substantially raises the free energy of the stalk (12). Models that allow for variation in lipid molecule tilt within the monolayers predict lower energies (1–4,25), because this permits the monolayers to form nonsmooth interfaces, which make these interstices unnecessary. Crudely, the monolayers can form ''joints'' at which the monolayer curvature makes a discontinuous change, as in the center of the stalk structure in Fig. 1 *A*. The curvature and tilt energy per unit area is then given by (11)

$$f_t = \frac{1}{2}k_m(\tilde{J} - J_s)^2 + \kappa\tilde{K} - \frac{1}{2}k_mJ_s^2 + \frac{1}{2}k_t(\bar{t}^2), \qquad (2)$$

where t characterizes the tilt of a molecule away from the local surface normal vector, and k_t is a tilt elastic constant. k_t cannot be measured directly. An estimate (26) of 0.001 k_BT/nm^2 was used in previous studies (2–4,11), although a more recent estimate (27) places the value at twice the original value. $\tilde{J}$ and $\tilde{K}$ are the splay and saddle splay, respectively, which include additive contributions from monolayer bending and tilt variation along the monolayer surface. In monolayers with vanishing tilt, these variables are the same as J and K, respectively, in Eq. 1. The values of k_m, J_s, and κ in Eq. 2 are assumed to have the same values as in Eq. 1, and these values are as measured via experiments on H_{II} and Q_{II} phases (see below). Thus, in the limit of zero tilt, Eq. 2 reduces to Eq. 1. A tilt model is not necessary to describe the curvature energies of catenoidal-fusion pore structures, because they lack hydrophobic interstices.

The curvature free energy of a fusion intermediate is the integral of Eq. 1 or Eq. 2 over the area of all the monolayer segments composing the structure. Let F be the total curvature energy of a segment of monolayer. F is the integral of f or f_t over the area, A, of a monolayer segment:

$$F = \int fdA = F_b + F_G, \qquad (3)$$

where F_B is the contribution of bending elastic energy and F_G is the contribution of Gaussian curvature elastic energy:

$$F_G = \kappa \int KdA. \qquad (4)$$

For the stalk, F_G and F_B are the area integrals of the second term, and of the sum of the other two terms, respectively, in Eq.2. For flat bilayers, $K = 0$ and $F_G = 0$.

What is F_G for the intermediates in membrane fusion?

For monolayers with smooth interfaces, the change in total area-integrated Gaussian curvature during fusion intermediate formation is determined by the change in topology of the system, including all the lipid monolayers (18). Formation of each stalk between the proximal monolayers of two liposomes changes the area integral of the Gaussian curvature of all the monolayers by -4π. Conversion of each stalk to a catenoidal fusion pore changes the total integrated Gaussian curvature by another unit of -4π.

However, the change in Gaussian curvature energy is determined by the change in the product of κ and the area integral of K for all monolayers in intermediate compositions (Eq. 4). κ is composition-dependent, and the composition can vary from place to place in a biomembrane, so the intermediate energy must be calculated with the local value of κ in each monolayer that forms the intermediate. Let $\kappa_{proximal}$ and κ_{distal} be the values of κ for the lipids in the proximal and distal monolayers, respectively. It is convenient to consider the case of intermediates forming between infinite flat sheets of membrane, since the original flat sheets have $K = 0$ and thus zero Gaussian

curvature energy. For the proximal monolayer of a stalk, $\int KdA = -4\pi$. The Gaussian curvature elastic energy of the stalk, F_G^{stalk}, is the sum of the contributions from the proximal and distal monolayers:

$$F_G^{stalk} = F_G^{proximal} + F_G^{distal}. \quad (5)$$

The integral $\int KdA$ for the distal monolayers of the stalk is 0. Thus, by Eq. 5,

$$F_G^{stalk} = \kappa_{proximal}(-4\pi) + \kappa_{distal}(0) = -4\pi\kappa_{proximal}. \quad (6)$$

HFs (3) are radially expanded stalks with a patch of flat bilayer inserted in the center (Fig. 1 *B*). Since the flat bilayer has zero Gaussian curvature, the F_G values for the proximal and distal monolayers are the same as in the stalk:

$$F_G^{HF} = F_G^{stalk} = -4\pi\kappa_{proximal}. \quad (7)$$

In the catenoidal fusion pore, the two planar distal monolayers of the original bilayers become continuous, as do the facing monolayers. If we assume that the proximal and distal monolayers have the same value of κ, then, by Eq. 4, the $\int KdA$ contribution of the distal monolayer is the same as for the proximal monolayer in the stalk:

$$F_G^{pore} = -4\pi(\kappa_{proximal} + \kappa_{distal}). \quad (8)$$

For monolayers with nonsmooth surfaces, like the proximal monolayer of the stalk in previous studies (2–4,11), tilt contributions to K can change the area-integrated value of K from the value in Eq. 6. However, at least in the case of Kozlovsky et al. (11), this makes only a small difference from the smooth monolayer value in Eq. 6: the Gaussian curvature energy of stalks is -11.8κ, which is only a 6% difference from -4π.

To what extent have values of κ been measured?

Recent measurements of the ratio κ/k_m in symmetric bilayers, which are accurate to within ~10%, have been obtained in only two lipid systems: glycerolmonooleate/DOPC/DOPE = 0.58:0.38:0.04, where the ratio is $\kappa/k_m = -0.75 \pm 0.08$ (17); and DOPE-Me (18,19), where the ratio is -0.83 ± 0.08 (18) or -0.90 ± 0.09 (19). The method used by Siegel (19) is slightly more accurate than that used by Siegel and Kozlov (18), for reasons discussed by Siegel and Tenchov (19,28). k_m was assumed to be 10 k_BT for DOPE-Me (18), so κ is ~ -9 k_BT for this lipid. As will be shown in the course of this work, κ is within <16% of the DOPE-Me value for at least three other lipid systems (DOPC, DOPE, and an equimolar DOPC/cholesterol mixture). It has been argued that for bilayer-forming lipids in general, κ/k_m must be > -1 (17) and < -0.5 (29). k_m for many biologically relevant lipid systems is on the order of 10 k_BT (29), which suggests that κ is usually in the range -5 to -10 k_BT. Therefore, assuming that the value of κ for the four lipids discussed in this work (-8 to -9 k_BT) is representative of most membrane lipids, we see from Eqs. 6–8 that the Gaussian curvature energy of fusion intermediates could range between 100 and 200 k_BT, which is obviously a very significant contribution. However, as discussed below, contributions of this magnitude are necessary to resolve paradoxes concerning lipid phase behavior that occur if κ is assumed to be 0, as in some previous calculations (1–4,14,25).

Estimating κ on the basis of observed lipid phase behavior

Lipid compositions with symmetric bilayers should form thermodynically stable catenoidal fusion pores and bicontinuous Q_{II} phases when the following inequality is satisfied (19):

$$\frac{\kappa}{k_m} \geq 2\delta J_s - \frac{\delta^2 J_s^2}{2}. \quad (9)$$

δ is the distance between the bilayer midplanes and the neutral plane of the lipid monolayers. It is assumed that the neutral plane is at the interface between the hydrophilic and hydrophobic regions of the monolayer. Using data from Rand and Parsegian (30) for monomethylated egg PE, δ is estimated to be 1.3 ± 0.1 nm. Using data from detailed structural studies of the DOPC L_α phase at 30°C (31), one obtains nearly the same value (1.36 nm). Hence, a value of 1.3 ± 0.1 nm is used here for dioleoyl-chain lipids and lipid compositions with similar average chain lengths.

The relationship in Eq. 9 is also applicable to lipid mixtures. If a lipid composition forms bicontinuous Q_{II} phases at equilibrium under given conditions, and one knows the values of k_m, J_s, and δ for the lipid composition of the Q_{II} phase, one can calculate a lower bound to the value of κ/k_m via Eq. 9. Conversely, if a Q_{II} phase is not observed, then Eq. 9 provides an upper bound to the value of κ/k_m. J_s of the lipid components decreases with increasing temperature. The temperature at which the curvature energies of the L_α and Q_{II} phases are equal is denoted as T_K (19), and is defined as the temperature at which the equality in Eq. 9 is satisfied. The value of κ/k_m at $T = T_K$ is designated M:

$$M = \left.\frac{\kappa}{k_m}\right|_{T=T_K} = 2\delta J_s - \frac{\delta^2 J_s^2}{2}. \quad (10)$$

The value of J_s can be measured by x-ray diffraction experiments on samples of the H_{II} phase of the lipid composition in the presence of long-chain alkanes (32). Knowing the values of J_s, k_m, and δ at T_K, one can determine the value of κ for the mixture. If we have expressions for the elastic constants of the mixture in terms of the elastic constants of the pure components, we can use Eq. 10 to estimate the Gaussian curvature elastic moduli of lipids that do not form Q_{II} phases by themselves. The values of κ and k_m are expected to change with temperature, but the ratio κ/k_m for DOPE-Me appears to be constant to within ~1% across a temperature interval of 35°C (19). The value of k_m for DOPE decreases linearly with increasing temperature by ~15% between 10°C and 60°C (33). Hence, the measured values of k_m and κ are fairly constant across small temperature intervals of a few tens of degrees.

We will only consider mixtures of two lipids for which δ is constant. Let the subscript α indicate the elastic constants of the ''host'' lipid. The subscript β indicates the elastic constants of the ''guest'' component, which is a small fraction of the total lipid. The J_s of the mixture may be expressed as the molecular-area-weighted sum of the spontaneous curvatures of the pure lipid constituents (J_α and J_β) (34):

$$J_s = y_\alpha J_\alpha + y_\beta J_\beta = (1 - y_\beta)J_\alpha + y_\beta J_\beta, \quad (11)$$

where the area fractions y_α and y_β can be calculated based on knowledge of the area/molecule of each of the two lipids at the neutral plane (a_α and a_β, respectively) and their mole fractions ($1 - x_\beta$ and x_β, respectively):

$$y_\beta = \frac{a_\alpha(1 - x_\beta)}{a_\alpha(1 - x_\beta) + a_\beta x_\beta}; \quad y_1 = \frac{a_\beta(x_\beta)}{a_\alpha(1 - x_\beta) + a_\beta x_\beta}. \quad (12)$$

The spontaneous curvature of binary lipid mixtures is often observed to be approximated by a mole-fraction-weighted sum of the spontaneous curvatures of the lipids (e.g., (35–39)). Equation 12 is a mole-fraction-weighted sum if the two lipid species have equal areas at the neutral plane ($a_\alpha = a_\beta$). The $a_\alpha \approx a_\beta$ condition is met by most of the lipids studied in (35–38). The J_s of a mixture may also seem linear in the mole fraction of β if $a_\alpha \neq a_\beta$, but the area fraction of β is kept small (37,39). Here, we will be concerned predominantly with DOPE and DOPC, which have similar values of area/molecule at the neutral plane (37), so $x_\beta \approx y_\beta$ (to within a few percent).

The bending elastic modulus of a two-component lipid mixture, k_{mix}, is given by (34)

$$\frac{1}{k_{mix}} = \frac{y_\alpha}{k_\alpha} + \frac{y_\beta}{k_\beta} = \frac{(1 - y_\beta)}{k_\alpha} + \frac{y_\beta}{k_\beta}, \quad (13)$$

where k_α and k_β are the bending moduli of the pure components. Finally, we need an expression for the monolayer Gaussian curvature elastic modulus of a two-component mixture in terms of the Gaussian moduli of the components. If one adds a term for the Gaussian curvature elastic energy to the expression for the free energy of a lipid monolayer, and performs the same analysis as in Kozlov and Helfrich (34), then the expression for the Gaussian curvature elastic modulus of the mixture is

$$\kappa = N_\alpha \left(\frac{\partial \kappa}{\partial N_\alpha}\right)_{A,N_\beta,J,K} + N_\beta \left(\frac{\partial \kappa}{\partial N_\beta}\right)_{A,N_\alpha,J,K}, \qquad (14)$$

where N_α and N_β are the number of molecules of species α and β per unit area, respectively; and A is the monolayer area. We assume that the contributions of the individual lipid species to κ do not depend on the lipid composition (ideal solution behavior). This is a good assumption for weakly interacting lipids, like PE and PC, but might be violated in mixtures with nonideal mixing behavior, like PC and cholesterol. With this assumption, for constant A and constant numbers of lipid molecules N_α and N_β,

$$\kappa = y_\alpha \kappa_\alpha + y_\beta \kappa_\beta = (1 - y_\beta)\kappa_\alpha + y_\beta \kappa_\beta. \qquad (15)$$

Expressing M for the two-component mixture (Eq. 10) in terms of Eqs. 11–15, rearranging and retaining terms only to the first power in y_β (since $y_\beta \ll 1$), one obtains

$$\kappa_\beta = k_\alpha \left[\frac{M}{y_\beta} + M_\alpha \left(2 - \frac{1}{y} - \frac{k_\alpha}{k_\beta}\right)\right], \qquad (16)$$

where $M_\alpha = \kappa_\alpha/k_\alpha$, the ''host'' lipid property that is measured directly by the method in the studies by Siegel and Kozlov (18) and Siegel and Kozlov (19).

THEORETICAL RESULTS

The Gaussian curvature elastic modulus of DOPE, κ_{DOPE}

A good estimate of κ_{DOPE} can be made on the basis of observed phase behavior. DOPE and DOPE-Me should have similar elastic constant values: the values of k_m for the two lipids are similar (18,19), and the H_{II} tube diameters at T_H are about the same (40,41). On these grounds, one would expect DOPE to form a Q_{II} phase upon heating, just as in DOPE-Me (20). This is not observed. Instead, DOPE in excess water forms H_{II} phases if heated through the lamellar (L_α)/inverted hexagonal (H_{II}) phase transition temperature (T_H), and only forms Q_{II} phases if the temperature is cycled back and forth across T_H, between −5°C and 15°C (42,43). Other pure PE systems behave similarly (44,45). This Q_{II} phase metastability in PE occurs because of the influence of the particularly strong attraction between L_α phase bilayers in pure PEs as compared to PE-PC mixtures or mono-methylated PEs. The energy of this interaction is absent in the Q_{II} phase, where bilayers are several times farther apart than in the L_α phase (28). This effect increases the L_α/Q_{II} phase transition temperature (T_Q) to be $\geq T_H$. However, the Q_{II} phase can form during temperature cycling: each time the system is cooled through T_H, most of the H_{II} phase lipid reverts to L_α phase, but a fraction enters the Q_{II} phase instead, and the Q_{II} phase is easily supercooled once it forms and also persists to temperatures $>T_H$ on reheating (20).

The total free energy of lipid in the Q_{II} and H_{II} phases, composed of curvature energy and bilayer-bilayer interaction energy contributions (28), must be equal at some temperature within the cycling interval. This condition is expressed as

$$f_Q = f_H + (g_H - g_u), \qquad (17)$$

where f_Q and f_H are the curvature free energies of the Q_{II} and H_{II} phases, respectively, with respect to planar bilayers, and g_u is the bilayer-bilayer interaction energy in the L_α phase. g_u is a large positive value for DOPE: work must be done to separate the bilayers in the L_α phase so that the Q_{II} phase can form. The lipid interfaces in the H_{II} phase of DOPE in excess water are two or three times farther apart than in the L_α phase, but there may be an interaction energy in this phase, g_H, whose form is not known. We presume that g_H is positive as well, but smaller than g_u, so that $0 \geq g_H - g_u \geq -g_u$.

Since the Q_{II} phase does not form before the H_{II} phase on slow heating, the temperature at which the condition in Eq. 17 is met must be $<T_H$, which is 3°C for DOPE (46). At T_H, $f_H = 0$, so at this temperature, the value of f_Q lies between two values: if $g_H - g_u = 0, f_Q$ has its maximum value of 0, which means that κ/k_m has the value given by Eq. 10. If $g_H - g_u < 0$, then $f_Q < 0$ and T_K is at a lower temperature than T_H. At the lower temperature of the cycling range, −5°C, the temperature is $<T_H$, and f_H is >0. f_H can be calculated at a temperature T in terms of the spontaneous curvature at T and T_H: $J_s(T)$ and $J_s(T_H)$ (18,47):

$$f_H(T) = \frac{k_m}{2}\left[(J_s(T_H))^2 - (J_s(T))^2\right]. \qquad (18)$$

We assume that J_s is equal to the the inverse of the pivotal plane radius (32). This radius has been measured in DOPE at only a few temperatures, mostly at or above room temperature (32,33,36,37,48). A consensus value of 2.85 nm at 22°C (36,37,48) is used. The radius decreases linearly with increasing temperature at a rate that is approximately −0.0109 nm/°C (33). With these values, the extrapolated values of J_s at −5°C and T_H are −0.318 nm^{-1} and −0.320 nm^{-1}, respectively. k_m for DOPE is 9 k_BT when corrected for the discrepancy between the neutral and pivotal planes (36). Thus, at −5°C, $f_H = 0.0261\ k_BT/nm^2$. g_u has been measured for egg PE and L_α phase POPE as 0.14 erg/cm^2 or 0.017 k_BT/nm^2 (30). With these values, it is clear that f_Q at −5°C is >0 for the entire range of values of $g_H - g_u$ considered here: it does not matter what the exact value of g_H is. According to the form of expression of the curvature energy of Q_{II} phases (18), if $f_Q > 0$ at a given temperature, then that temperature is $<T_K$, and for DOPE, $-5°C < T_K \leq 3°C$. Then, according to Eq. 10, M is in the range −0.941 to −0.912, and a value of -0.927 ± 0.015 is used here. The standard errors in the values of the bending elastic moduli are assumed to be ±10%, which is approximately the uncertainty cited in other studies (36,37,48); the errors in the spontaneous curvatures are ±3% (corresponding to an error in neutral plane placement of ±0.1 nm for lipids like DOPE and DOPE-Me, which is a typical

error in such x-ray diffraction experiments); and the error in δ is ± 0.1 nm. The error in δ is estimated from the difference in values obtained for monomethylated egg PE and DOPC near room temperature (30,31). Therefore, according to Eq. 10, $\kappa_{DOPE} = -8.3\ k_BT \pm 1\ k_BT$, where the uncertainty arises from the uncertainty in δ, k_m, and $J_s(T_K)$.

The Gaussian curvature elastic modulus of DOPC, κ_{DOPC}

κ_{DOPC} can be determined from the phase behavior of DOPE/DOPC mixtures using Eqs. 10–16 and the value of κ_{DOPE} estimated above. Ideally, one would determine the value of M of a DOPE/DOPC mixture by measuring the temperature dependence of the unit cell constant of the Q_{II} phase (19). However, a good estimate can also be derived from the temperature at which isotropic ^{31}P NMR resonances are observed. In a dispersion of large multilamellar liposomes of phospholipids, isotropic ^{31}P NMR resonances arise from Q_{II} phases, or the catenoidal fusion pores that are Q_{II} phase precursors (18,19). This correspondence of the appearance of isotropic ^{31}P-NMR resonances with Q_{II} phase formation has been verifed via x-ray diffraction for DOPE-Me (20,40,49), DEPE and DOPE exposed to temperature-cycling protocols (42–45), and soy PE/egg PC (50). As a function of increasing temperature, the curvature energy of catenoidal fusion pores first becomes equal to that of the L_α phase at T_K. Hence, the temperature at which the isotropic component becomes dominant in the ^{31}P NMR spectrum of a phospholipid mixture is an estimate of T_K.

The relationship between the temperature at which isotropic ^{31}P NMR resonances appear and T_K is approximate, however. The curvature energy of catenoidal fusion pores is small and changes slowly with temperature at temperatures near T_K (18,19), so that some of these structures form at temperatures a few degrees below T_K. For example, isotropic resonances in DOPE-Me dispersions have been observed starting at temperatures between 10° below T_K (49,51–53) and T_K (54–56), where T_K was later determined via x-ray diffraction (19,20).

^{31}P NMR spectra of 4:1 (mol/mol) mixtures of DOPE/DOPC show an isotropic component at 35°C (49), and the spectrum is almost completely isotropic after prolonged incubation at 40°C (57). The J_s and k_m of DOPC were measured as -0.115 nm^{-1} and 9 k_BT, respectively, at 32°C (37). Thus, 40°C is an estimate of T_K for the lipid mixture, and the area/molecule values of DOPE and DOPC at the neutral plane are assumed to be equal. The difference between J_s of DOPC between 32 and 40°C is negligible. The value of J_s for DOPE at 40°C is estimated to be -0.377 nm^{-1}. For $y = 0.2$ and $k_{DOPE} = k_{DOPC}$, Eq. 16 reduces to the simpler form $\kappa_{DOPC} = k_{DOPE}(5M - 4M_{DOPE})$. The value of κ_{DOPE} calculated above is used to calculate M_{DOPE} (Eq. 10). When the relative standard errors assumed are the same as in the calculation of κ_{DOPE}, with Eqs. 10–16, one obtains $\kappa_{DOPC} = -7.6 \pm 1.5\ k_BT$.

The Gaussian curvature elastic modulus of DOPC/cholesterol = 1:1, $\kappa_{PC\text{-}CH}$

It was recently shown that an equimolar mixture of DOPC and cholesterol forms a Q_{II} phase in excess water starting at ~65°C (58). As noted by Tenchov et al. (58), 65°C is an upper bound to T_K. The J_s values for DOPC/cholesterol mixtures were measured at 32°C in Chen and Rand (37) by adding tetradecane to induce an H_{II} phase in the DOPC/cholesterol mixtures, and then measuring the change in the H_{II} phase unit-cell dimension under osmotic stress (32). If we use Chen and Rand's (37) data to approximate J_s as the inverse of the pivot plane radius in the H_{II} phase in the DOPC/cholesterol = 1:1 system, we find that at 32°C, $J_s = -0.25$ nm^{-1}. k_m for this mixture is 11 k_BT (37). Since J_s decreases with increasing temperature, J_s for the system at 32°C will be smaller (more negative) than the value at 65°C. If the T_K of the mixture is 65°C and the temperature dependence of J_s for the DOPC/cholesterol mixture is the same as for DOPE-Me (18), this would make the value of J_s 16% smaller, or -0.29 nm^{-1}, at 65°C. Therefore, we use a value of J_s at $T_K = -0.27 \pm 0.02$ nm^{-1}. Assuming the same uncertainties in k_m and δ as above, with Eq. 10, one obtains $\kappa_{PC\text{-}CH} = -8.4 \pm 1.1\ k_BT$.

The estimated values of κ of the three representative lipid systems are given in Table 1, along with the values of k_m and J_s for $T = 32$°C.

Effect of Gaussian curvature elastic energy contributions on fusion intermediate energies

The discussion here will concentrate on the model for stalk energies of Kozlovsky et al. (11), because more analytical expressions for the dependence of stalk curvature energy on curvature elastic constants are given in that case than in the study by May (4). However, as will be shown below, addition of a Gaussian curvature elastic energy to the energy reported in the study by May (4) will make the stalk energy comparable to or larger than the similarly adjusted values predicted by the theories in other studies (1–3).

The curvature elastic energy of a stalk in excess water, F_s, according to the model of Kozlovsky et al. (11) is given by

TABLE 1 Curvature elastic constants for the lipid compositions

Lipid system	κ* (k_BT)	k_m (k_BT)	J_s at 32°C (nm^{-1})
DOPE	-8.3 ± 1	9†	-0.365†
DOPC	-7.6 ± 1.5	9‡	-0.115‡
DOPC/cholesterol = 1:1 mol/mol	-8.4 ± 1.1	11‡	-0.250§

*Calculated as described in the text.
†Calculated from data in other studies (33,36,37,39), as described in the text.
‡Value from Chen and Rand (37).
§As calculated via Eqs. 11 and 12 using values of J_s for DOPC and cholesterol from Chen and Rand (37).

$$F_s = F_s^0 + 26.1\, k_m \delta J_s - 11.8\kappa, \quad (19)$$

where F_s^0 is the splay elastic energy necessary to create a stalk in a lipid system with $J_s = 0$, which is a constant equal to $\sim 81\ k_BT$. This value of F_s^0 is appropriate for stalks forming between the membranes of two isolated vesicular membranes, as in biomembrane fusion or the fusion of small liposomes, where the membranes around the periphery of the stalk are separated by a distance of >3 nm (11). F_s^0 is larger if this distance is smaller: for example, if the interbilayer separation is 2 nm, $F_s^0 \approx 90\, k_BT$ (11). In Kozlovsky et al. (11) the contributions to the curvature elastic energy are due to splay (a combination of monolayer bending and gradients in lipid molecule tilt) and saddle splay (Gaussian) curvature elastic energy. These are given by the sum of the first two terms on the righthand side of Eq. 19, and the last term, respectively. The contribution of tilt elastic energy (the last term in Eq. 2) is contained within the value of F_s^0.

Next, the curvature elastic energy of the catenoidal fusion pore is evaluated. In Siegel and Kozlov (18), it was shown that fusion pores will have catenoidal profiles for membranes in which the two monolayers have the same composition. The catenoid is a surface with zero mean curvature. The catenoidal surface is the bilayer midplane. The curvature energy of the monolayers making up the catenoidal fusion pore is not zero, however, because the neutral planes of the monolayers do not lie on the catenoid surface, but lie on surfaces that are displaced from the bilayer midplanes, and these surfaces have nonzero curvature energy. A model has been developed for the curvature energy of catenoidal fusion pores and Q_{II} phases that is accurate to the fourth order in curvature (19). However, here the fusion pore energy is calculated using the second-order curvature energy model in Siegel and Kozlov (18) to be consistent with the second-order calculation for stalks (Eq. 19). For symmetric bilayers, the curvature elastic energy of a catenoidal fusion pore is given by

$$F_{pore} = 16\pi\left(k_m \delta J_s - \frac{\kappa}{2}\right). \quad (20)$$

The contribution of Gaussian curvature elastic energy is $-8\pi\kappa$ (Eq. 8). If a catenoidal fusion pore forms between flat bilayers, there must be a region with nonvanishing curvature around the periphery of the pore, which will also contribute to the curvature energy. However, these contributions are small compared to k_BT for big enough patches of fusing membranes (59). Moreover, if the catenoidal fusion pore forms between two bilayer membranes that each have even slight nonzero convex curvature, as in the fusion of an intracellular secretory vesicle with a slightly invaginated segment of a cellular plasma membrane, or the fusion of two unilamellar liposomes, then there is no such additional contribution to F_{pore}; there will generally be a finite radius from the axis of the catenoidal fusion pore at which the tangent angle of the pore membrane is equal to the tangent angle of the surrounding liposomal membrane, as long as the pore radius is smaller than the vesicle radius. Hence, the contribution from the peripheral regions can be neglected in Eq. 20.

The total curvature elastic energy of stalks and catenoidal fusion pores, along with the contributions from the splay and saddle splay terms for stalks, and the bending and Gaussian curvature elastic terms for catenoidal fusion pores, can be calculated with the values of the elastic constants in Table 1, using Eqs. 8, 19, and 20. These values are displayed in Table 2. The uncertainties in the energies given in Table 2 are only the uncertainties introduced by the uncertainties in the values of κ for each lipid composition (Table 1). They do not take uncertainty in the values of any other variables into account. The intermediate curvature energies can also be calculated for mixtures of DOPE and DOPC using the elastic constants for each of the pure lipids and Eqs. 11–13 and 15. The results of these calculations are displayed in Fig. 2.

The bending energy values for stalks in Table 2 correspond to the curvature energies one would calculate with $\kappa = 0$. The dependence of the stalk bending energies on J_s is similar to the dependence of the stalk energies found via the model of May (4), which were also calculated with $\kappa = 0$. However, the energies in that study (4) are higher for small J_s and lower at J_s values closer to 0. The stalk bending energy for the J_s of DOPE would be ~ 0 (Fig. 7 in May (4)), and for DOPC ($J_s = -0.115\ nm^{-1}$) $\sim 20\ k_BT$. These values are $\sim 30\ k_BT$ higher and $\sim 26\ k_BT$ lower, respectively than the values for DOPE and DOPC in Table 2 of this article. A Gaussian curvature elastic contribution must be added to the energies calculated by May (4). This contribution would be $\sim 100\ k_BT$ for both lipids (Eq. 6). With this contribution, the total stalk energy for the May model (4) would be $\sim 100\ k_BT$ for DOPE and 120

TABLE 2 The curvature elastic energy of stalks and fusion pores (in k_BT)

	Stalk			Fusion pore		
System	Saddle splay	Splay	Total	Gaussian	Bending	Total
DOPE	98 ± 12	−30	68 ± 12	209 ± 25	−215	−6 ± 26
DOPC	90 ± 18	46	136 ± 18	191 ± 38	−68	123 ± 38
DOPC/cholesterol = 1:1 mol/mol	99 ± 13	−12	87 ± 13	211 ± 27	−180	31 ± 27

Values were calculated using the elastic constant values in Table 1. Stalk splay and saddle splay curvature energies were calculated using Eq. 19. The splay and saddle splay elastic energies of stalks are the sum of the first two terms, and the last term, respectively, in Eq. 19. Fusion pore Gaussian curvature elastic energies were calculated using Eq. 8; and the total curvature energies using Eq. 20. The indicated uncertainties in total energy are the uncertainties introduced by the uncertainty in κ for each system (Table 1).

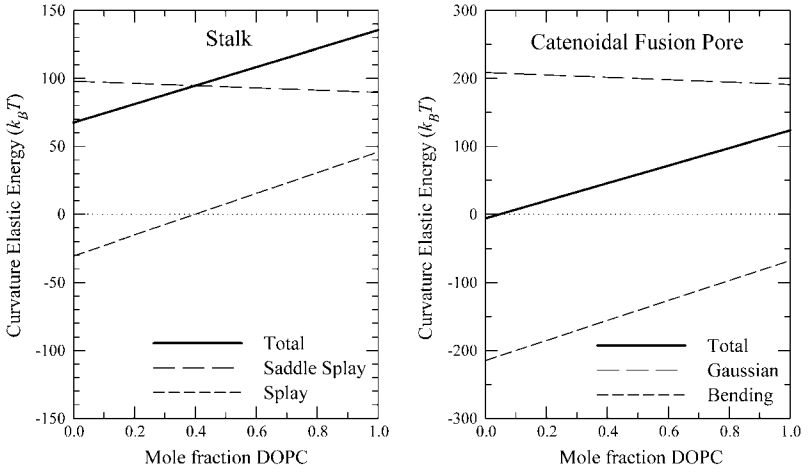

FIGURE 2 Plot of the curvature elastic energy of stalks (*left*) and catenoidal fusion pores (*right*) in DOPE-DOPC mixtures as a function of the mole fraction of DOPC in the mixture. Solid lines represent the total curvature elastic energy, long-dashed lines the splay elastic or bending elastic energy for stalk or catenoidal fusion pore, respectively, and short-dashed lines the saddle splay or Gaussian curvature elastic energy for stalk or catenoidal fusion pore, respectively.

k_BT for DOPC. However, these are approximate comparisons. A smaller value, $k_m = 6.8\ k_BT$, was used by May (4), and a different energy optimization procedure was applied than in Kozlovsky et al. (11). For example, the monolayer thickness was taken as another degree of freedom in May (4). To better compare the two models, the stalk energies should be recalculated using the same values for the elastic constants, the values of κ estimated here, and the optimization procedure described in May (4).

DISCUSSION

The values of κ for the different lipid compositions are similar (Table 1), and similar to the value measured for *N*-monomethylated DOPE (19), despite the large uncertainty in the calculations. This may not be surprising in light of the similarity in the values of k_m for the same lipids. The Gaussian curvature elastic energies for stalks and catenoidal fusion pores are large and positive for all the lipid compositions (Table 2, Fig. 2), and are frequently larger in absolute magnitude than the contributions from bending or splay elastic energy.

The data in Fig. 2 also show that intermediate energies that include the Gaussian (saddle splay) curvature elastic contribution are consistent with observed lipid phase behavior in excess water. First, the total stalk curvature energies are >0 for DOPE, DOPC, and their mixtures (Table 2 and Fig. 2). This is compatible with the absence of any rhombohedral phases in excess water in these compositions (60). In contrast, if $\kappa = 0$ in Eq. 19, as in Kozlovsky and Kozlov (2), and the only contribution to the total curvature elastic energy is from splay, then Eq. 19 would predict the existence of thermodynamically stable stalks in excess water in DOPE-DOPC mixtures near room temperature for mixtures with <40 mol % DOPC (Fig. 2 *left*, *long-dashed line*). Rhombohedral phases composed of stalks are observed in DOPC and in DOPE-DOPC mixtures (60), but not in pure DOPE, and only if the lipids are extensively dehydrated to water activities of 0.4–0.8. Extensive dehydration lowers the amount of energy necessary to create stalks from the L_α phase: dehydration forces bilayers into closer proximity against strong repulsive forces, whereas rhombohedral phase (stalk) creation from the L_α phase destroys the bilayer/bilayer interface (11).

Second, the total curvature energy of catenoidal fusion pores is close to zero for DOPE and for mixtures of DOPE with small mole fractions of DOPC (Table 2 and Fig. 2). This is compatible with the isotropic ^{31}P NMR resonance observed for DOPE-rich mixtures of these lipids at 40°C, close to the temperature used for our calculations (49). The catenoidal fusion pore energy is also low for DOPC/cholesterol = 1:1 (Table 2), which is compatible with the formation of a Q_{II} phase at a higher temperature (~65°C (58)). In Fig. 2, the total curvature energy of a catenoidal fusion pore increases as the mole fraction of DOPC increases in a DOPE-DOPC mixture, consistent with the observation that the temperatures at which Q_{II} phases and Q_{II} phase precursors appear increase with increasing mole fraction of DOPC in DOPE (49). In contrast, if $\kappa = 0$ in Eqs. 10 and 20, then catenoidal fusion pores would form a thermodynamically stable phase in all the lipid compositions treated in this work, and in fact in any lipid composition with $J_s < 0$ (like pure DOPC), which is not observed.

Comparison of predicted stalk energy with the rates of stalk-mediated processes in pure lipid systems

The curvature energies must not make the activation energy for formation of fusion intermediates so high that they cannot form at the rates of observed fusion processes. Lipid mixing and fusion between lipid vesicles are examples of processes that are thought to be stalk-mediated. In all the cases in Table 2 and Fig. 2, the curvature energy of the catenoidal fusion pores is less than the curvature energy of the stalks. This suggests that the energy barrier to stalk creation is the primary barrier to fusion in pure lipid systems. To minimize the

number of assumptions about the kinetic scheme for interconversion of fusion intermediates (e.g., reversible versus irreversible reactions, existence of side reactions, etc.), rate estimations will only be made for stalks.

To make order-of-magnitude estimates of the effects of intermediate energy on the rate of stalk-mediated processes without detailed knowledge of the kinetic scheme for intermediate formation, further simplifying assumptions are necessary. First, we assume that formation of the intermediate is a simple one-step process. In reality, processes like close opposition of two membranes may have to precede formation of a stalk structure between them. However, it was recently proposed that the membranes first come into contact via a stalklike deformation of one of the opposed membranes, and that the energy of this deformation is lower than that of the resulting stalk (61). Hence, the membrane-membrane contact and intermediate formation step might be treatable as a single process.

Second, it is assumed that the total curvature elastic energy of the stalk with respect to flat bilayers is a lower-bound estimate to the total activation energy for formation of the intermediate, W. With these assumptions, we can use an equation for estimating the order-of-magnitude waiting time, τ, for formation of stalk intermediates that was proposed by Weaver and Mintzer (62) and Kuzmin et al. (25):

$$\tau \approx \frac{\exp(W/k_BT)}{\omega SN}. \quad (21)$$

S is the area/fusion site, and N is the number of possible fusion sites. ω is the characteristic frequency of fluctuations within lipid monolayers, which is taken to be 10^{11} s^{-1} nm^{-2} (62). We consider the area of interaction between a unilamellar liposome with a radius of 50 nm and another membrane. It is assumed that the area of membrane-membrane contact is a disk with diameter equal to one liposome radius, so the contact area is $\pi(50\ \text{nm})^2$. The area of interface that can form a stalk is $\pi(3\ \text{nm})^2$, so the number of possible stalk initiation sites is $(50\ \text{nm})^2/(3\ \text{nm})^2$, and $SN = 8 \times 10^3$ nm^2. It is emphasized that Eq. 21 is only intended to yield estimates that are accurate to within a few orders of magnitude.

First, let us consider the rates of processes in protein-free lipid systems. Time-resolved cryoelectron microscopy experiments have shown that large unilamellar vesicles (LUVs) composed of egg PE or DOPE-Me fuse extensively within 16 ms when subjected to a temperature jump to $T > T_H$ (21). Using $W = 68\ k_BT$ for pure DOPE (Table 2), we find $\tau \sim 10^{14}$ s for stalk formation. The stalk energy for DOPE in Table 2, and hence W, has an uncertainty due to uncertainty in κ of 12 k_BT, which makes τ uncertain to within a very large factor of 10^5. Even so, a figure of $\tau \sim 10^{14}$ s indicates that the model for the curvature energy of stalks in Kozlovsky et al. (11) yields values that are obviously too large to be compatible with the observations in Siegel et al. (24). The estimated value of τ suggests that the model used here (11) overestimates the stalk curvature energy by $\sim 30\ k_BT$ or more.

The L_α/H_{II} transition in the bulk L_α phase is also thought to begin with stalk formation (3,14,63). Significant numbers of stalks must form on timescales shorter than the half-time of the transition. In PE L_α phases, in which the water/bilayer interfaces are ~1–1.5 nm apart (30), the appropriate value for formation of stalks (F_s^0 in Eq. 19) is $\sim 95\ k_BT$ (11). This value of F_s^0 includes the effect of constraints on the shape of the stalk due to repulsive forces between adjacent membranes in the multilayer stack. With this value of F_s^0, the total energy of stalks forming within a bulk L_α phase of DOPE would be $\sim 82\ k_BT$ (Eq. 16). A 10-μm cube of L_α phase (chosen to represent an average multilamellar liposome) contains $\sim 8 \times 10^9$ fusion sites if we use the same value of S as before. With these values, Eq. 21 predicts a waiting time for formation of even a single stalk in an MLV of 10^{15} s. Even with an uncertainty in W of 12 k_BT, this very long waiting time is incompatible with measurements of the L_α/H_{II} transition rate in DOPE MLVs. The L_α/H_{II} transition has a half-completion time of several tens of seconds or less when a sample is superheated by $\geq 5°$ (64), and ~1 s when samples are superheated by 30° (65). This discrepancy suggests that the stalk curvature energy estimated by the model in Kozlovsky et al. (11) is too high by $>30\ k_BT$; a result similar to our estimate for fusion in unilamellar liposomal systems. The stalk model in May (4) seems to generate an even higher total stalk curvature energy for the DOPE system, but as noted in the Theory section, more detailed calculations would be required to test this.

The total stalk curvature energy in DOPC is estimated to be $136 \pm 18\ k_BT$ (Table 2). With this value of W, $\tau \sim 10^{44}$ s. According to this estimate, DOPC LUVs should not fuse with each other in excess water. This is certainly compatible with their observed stability in excess water and the fact that they remain stable even if a quite substantial stress is applied via suspension in 10% PEG (66). The PEG concentration required to induce fusion in small unilamellar vesicles composed of PE and PC mixtures increases with increasing PC content (67), as one would expect if the energetic barrier to membrane fusion increased with increasing PC content (Fig. 2). Thus, the energy predicted via Eq. 20 is consistent with observations for DOPC liposome fusion in the sense that DOPC liposome fusion is extremely slow or absent in excess water, and that the energy needed to create a stalk decreases with increasing PE content. The total stalk energies estimated for DOPC according to the May model (4) are also consistent with this conclusion.

In summary, the curvature energies of stalks calculated as in Kozlovsky et al. (11) are too large to be compatible with observed rates of lipid mixing and fusion in LUVs of pure DOPE (24), or with the observed rates of L_α/H_{II} phase transitions in DOPE (64,65). Assuming that vesicle fusion and the L_α/H_{II} transition are stalk-mediated, the model in Kozlovsky et al. (11) seems to overestimate the energy by 30 k_BT or more. Similar differences are found for the May theory (4). Discrepancies of this size may be due to such factors as a

difference between the estimated versus actual value of k_t or to gaps in the theories that have not been identified. It should also be pointed out that the expression for the stalk curvature energy in Eq. 19 contains the difference between a large positive contribution (the first and last terms) and a negative contribution that is similar in absolute magnitude (the second term). Hence, especially for lipids with low J_s, like DOPE, part of the apparent discrepancy in total energy may be the result of inaccuracies in the values of the elastic constants in the respective terms. The Kozlovsky et al. theory (11) rationalizes many qualitative and semiquantitative observations of lipid mixing and membrane fusion in pure lipid systems, such as the effects of lipid composition and bilayer composition asymmetry (5–9). It is important to note that the predicted stalk and catenoidal fusion pore energies are now consistent with observed lipid phase behavior, and that the apparent discrepancy in stalk energy estimated here is considerably smaller than those calculated using early stalk models (14), which was later referred to as the ''energy crisis'' (2). With inclusion of saddle splay and Gaussian curvature elastic energies, models of fusion intermediate energy (11,19) begin to pass the two tests proposed in the Introduction for models of fusion mechanisms. These models are accurate enough to make semiquantitative predictions about how proteins mediate biomembrane fusion. The models might be refined further by more detailed tests of predictions concerning rhombohedral (R) and Q_{II} phase stability, and by further consideration of the effects of local variations in lipid monolayer thickness (4).

The intermediate energies in this work were calculated using a continuum theory that was derived for systems with radii of interfacial curvature that are much larger than molecular dimensions (13). The radii of curvature of the stalk monolayers are comparable to or even smaller than lipid molecular dimensions, especially at the ''waist'' of the stalk (Fig. 1 *A*). As noted in Kozlovsky and Kozlov (2), the theory in Helfrich (13) successfully predicted the curvature energies in H_{II} phases with similarly small radii of interfacial curvature (36,47,68,69). However, the interface in the H_{II} phase has no Gaussian curvature. There is an apparent discrepancy between the stalk energies calculated in this work and the energies that are consistent with the observed rates of stalk-mediated processes. Perhaps some or all of this discrepancy is due to a failure of the continuum model to correctly estimate the curvature energies of surfaces with large geometric and Gaussian curvatures. One way to test this would be to determine whether models based on the continuum theory (13) accurately describe the stability of rhombohedral phases as a function of water activity, lipid composition, and temperature. A previous theoretical study of rhombohedral phase stability (11) could not unambiguously resolve this issue, in part because the rhombohedral phases in question only form at water activities of 0.4–0.8 (60). As noted in Kozlovsky et al. (11), the elastic constants (k_m, J_s, κ) are determined by separate experiments on systems at near unit water activity. The actual values of these constants may be different in such extensively dehydrated systems. The best test would be to apply the theory in Kozlovsky et al. (11) to rhombohedral phases that form at water activities closer to unity. There is preliminary evidence that some lipid compositions form at least some rhombohedral phase at a water activity of 0.9 (H. W. Huang, Department of Physics and Astronomy, Rice University, 2008, personal communication).

Estimated lipid intermediate energies for biomembrane fusion

Estimating the energy required to form fusion intermediates in a biomembrane lipid composition may give us insight into the mechanism of fusion. If the energy of a pure lipid fusion intermediate is too high for the intermediate to form at rates similar to biomembrane fusion, the discrepancy can be assigned to a difference in fusion mechanism relative to the mechanism corresponding to formation of the pure lipid intermediate; to a discrepancy in the model for calculating the energy of the lipid intermediate; to the effects of fusion proteins on intermediate energy; or to some combination of these possibilities. For the purposes of the calculations here, it is assumed that the stalk-HF-catenoidal fusion pore progression in a patch of membrane lipid is the basis of protein-mediated membrane fusion. We consider three illustrative cases; influenza virus lipid mixing with protein-free liposomes, exocytosis at central nervous system synapses, and fusion of sea urchin cortical granules.

The lipid compositions of the two lipid monolayers of biomembranes are generally different. It is important to estimate the effect of the differences in the elastic constants between the two monolayers on fusion intermediate energy. The expression for the curvature energy of the stalk (Eq. 19) was derived for symmetric-bilayer compositions. However, the splay elastic energy of the stalk is insensitive to the value of J_s of the distal monolayer (2), and most of the change in curvature is concentrated in a small area of opposed monolayer area. The opposed monolayers are the only ones that undergo a topological change, and thus the only ones that make a substantial contribution to the change in saddle splay (Eq. 6). Thus, it is a reasonable approximation to use Eq. 19 to estimate the curvature energy of stalks in asymmetric bilayers, using the elastic constants corresponding to the lipid composition of the opposed monolayers. The bending energy of catenoidal fusion pores is sensitive to the elastic constants of both monolayers (1).

Influenza virions have lipid compositions resembling raft microdomains (70). Cholesterol is ~44 mol % of the membrane. The phospholipid composition is about equally divided between three lipid classes: PE; a combination of PC and sphingomyelin; and acidic lipids (phosphatidylserine and phosphatidylinositiol). More than 60% of the phospholipid acyl chains are saturated (71). Phosphatidylcholine is concentrated in the external leaflet of the virus, as it is in the host cell from which the virus buds (72). The high proportion of

saturated acyl chains and the high combined PC and sphingomyelin content probably make both k_m and J_s for the external leaflet of the viral membrane larger than for the DOPC/cholesterol = 1:1 case in Table 2. k_m is probably greater than for pure DOPC due to the large proportion of saturated acyl chains, but the high cholesterol content could make J_s considerably less than for pure DOPC. However, if the viral membrane separates into liquid ordered and disordered phase regions, we cannot be sure which phase is most relevant for fusion activity. Hence, the patches of membrane that actually fuse might be lower in saturated chain lipids and cholesterol than the bulk composition. As for the influence of the external leaflet of the target liposomes, the lipid composition of the target liposomes did not have much effect on the overall rate of lipid mixing under the conditions used in other studies (73–76). In fact, the target membranes were >90 mol % DOPC in many cases (73–76), and the balance was ganglioside or glycophorin, which were added to act as receptors for the viral hemagglutinin. This suggests that the average of the lipid compositions of the viral and target membranes under these circumstances corresponded to a liquid disordered phase (e.g., enriched in DOPC). Therefore, it is assumed that the curvature energies of purely lipidic stalks for the influenza virus/DOPC LUV system lie between the values for DOPC/cholesterol and pure DOPC calculated in Table 2. The typical half-times for lipid mixing reported in other studies (73–76) were tens of seconds. Using the value of $SN = 8 \times 10^3$ nm^2 for interaction of vesicles of radius 0.1 μm, as estimated above, it is seen that to have $\tau \approx 1$ s in Eq. 21, W must be $<37\ k_BT$. The curvature elastic energy of stalks in DOPC/cholesterol = 1:1 is 87 ± 13 k_BT, and the value for DOPC is 136 ± 18 k_BT. This suggests that influenza-virus-induced lipid mixing could only proceed via lipidic stalk intermediates according to the model in Kozlovsky et al. (11) if the proteins perform functions corresponding to a reduction in W of 50–100 k_BT. Note that this estimate for the required effect of proteins on W may be decreased by the discrepancy in predicted versus observed lipidic stalk energy estimated above.

In the case of synaptic vesicle/plasma membrane fusion, the compositions of the external leaflet of the synaptic vesicle membrane and of the synaptic plasma membrane are taken to be similar (77). The synaptic vesicle membrane composition (78) consists of approximately equal weights of cholesterol and phospholipid, with a combination of PE and plasmenyl-PE representing 42 mol % of the phospholipid, PC and sphingomyelin representing 43 mol %, and PS 12 mol %. A large fraction of the acyl chains of the phospholipids are highly unsaturated, especially for the PE fraction. Since the combined fraction of high-curvature lipids (PE, plasmenyl PE, and cholesterol) is high and the acyl chains are extensively unsaturated, and PE is enriched in the external leaflet of synaptic vesicle bilayers (79) and in the cytoplasmic leaflet of plasma membranes, it is possible that the J_s for the two opposed monolayers is intermediate between that of pure DOPE and DOPC/cholesterol = 1:1. Synaptic vesicles are ~40 nm in diameter, and the lengths of the SNARE complex components are of order 10 nm (78), which suggests that there may be only one fusion site available per docked vesicle. In this case, $SN \approx 30$ nm^2. The time constant for release of the readily-releasable pool of synaptic vesicles is 2–4 ms when Ca^{2+} influx is not rate-limiting (80,81). Using a waiting time of 1 ms, one finds, via Eq. 21, that W must be $<22\ k_BT$. The total curvature energies of stalks in pure DOPE and equimolar DOPC/cholesterol are 68 ± 12 k_BT and 87 ± 13 k_BT, respectively (Table 2). This suggests that the protein fusion ''machinery'' has to perform functions corresponding to a reduction in W of 50–70 k_BT for fusion to occur on physiological timescales via formation of stalks, as described in Kozlovsky et al. (11). As with influenza hemagglutinin-mediated fusion, this estimate for the required effect of proteins on W may include the apparent discrepancy in lipidic stalk energy estimated here.

Sea urchin cortical vesicles (CVs) undergo fusion in a calcium-dependent manner (82,83). The lipid composition of the membranes of these vesicles (84) is somewhat similar to that of synaptic vesicles (SVs), and CVs and SVs have about the same weight ratio of cholesterol to phospholipid, although in CVs, PE represents a smaller fraction of the phospholipids, and there is almost no sphingomyelin. In addition, CV membranes seem to contain high levels of triacylglycerols (23% of the total lipid), and lower levels of monacylglycerols, free fatty acids, and lyso-PE. It is difficult to assess the influence of these latter compounds. However, we proceed by making the same assumption as for SVs, that the elastic constants for the two opposed monolayers in the CV system are intermediate between those of pure DOPE and DOPC/cholesterol = 1:1. CVs are ~1 μm in diameter (85), so we assume a contact-area diameter equal to one vesicle radius, and calculate SN in Eq. 21 to be $\sim 2 \times 10^5$ nm^2. The initial rate of CV fusion upon exposure to Ca^{2+} is on the order of 100%/s (83), so τ must be ~0.1 s. For this value of τ, W must be $<35\ k_BT$. This is ~30 and 50 k_BT smaller, respectively, than the total curvature energy of stalks in the pure DOPE and DOPC/cholesterol systems. This estimate is similar to that for SV/plasma membrane fusion, above, except that the fusion-mediating proteins in CV would have to reduce W to a slightly smaller extent for the stalk formation rate to correspond to the observed fusion timescale.

The stalk-pore theory is successful in explaining many qualitative features of biomembrane fusion (5–9), including recent observations of the effects of several exogenous lipids on biomembrane fusion rates (82) and the effects of exogenous cholesterol (83,86). Cholesterol increases the rate of exocytosis in sea urchin cortical granule fusion (83) and of hemifusion in hemagglutinin-induced cell fusion (86), and also promotes fusion pore opening in the latter system. These two roles are consistent with the expected reduction in stalk and HF energy by a lipid with such a negative value of J_s (37), and with the observed role of cholesterol in stabilizing

catenoidal fusion pores and Q_{II} phases (58). It is likely that intermediates resembling stalks mediate biomembrane fusion. However, as estimated above, it appears that the curvature energies of purely lipidic stalks are too high, by 30–100 k_BT, to be compatible with the observed rate of stalk-mediated processes in biomembranes. Part of this discrepancy may be due to inaccuracies in calculating the energy of lipidic stalks, since the energies for lipidic stalks, at least for PE, appear to be 30 k_BT or more too high. The balance of the apparent discrepancy in stalk energy in biomembrane systems (as much as 70 k_BT, depending on the system and the assumptions) must be due to some influence of the fusion-mediating proteins. How can fusion-mediating proteins reduce the energy of the first fusion intermediates in the context of the stalk model?

Can fusion-mediating proteins in vivo increase the rate of formation of lipid fusion intermediates by changing the local curvature elastic constants of lipid monolayers?

Proteins can impose membrane curvature that favors intermediate formation in at least three ways: scaffold creation, local modification of spontaneous curvature, and induction of bilayer asymmetry (see (6,87–89) for reviews). In modification of the local spontaneous curvature, protein moieties bind to the lipid-water interface, insert between the lipid headgroups, and impose a curvature on a small patch of the interface (88). In particular, Martens et al. (90) recently proposed that insertion of synaptotagmin C2 domains into the plasma membrane drives stalk formation by inducing a positive spontaneous curvature in an annulus of monolayer surrounding the monolayer patch that forms the stalk. It is postulated that this dimples the plasma membrane toward the synaptic vesicle membrane, and also places the central patch of monolayer that forms the stalk under positive curvature stress, so that its curvature energy is closer to that of a stalk. In Martens et al. (90), it was estimated that synaptotagmin binding could reduce the stalk energy by $\sim 20\ k_BT$.

In principle, moieties of fusion-mediating proteins can also bind to the opposed monolayer interfaces that form the stalk. Most of the fusion-mediating machinery is in the cytoplasmic space in synaptic vesicle fusion, and outside of the virions in influenza virus fusion. Moreover, the area of monolayer involved in stalk formation is not large, and few peptide-lipid interactions would be required. The area of opposed monolayer in either membrane that participates in stalk formation is $\sim 30\ nm^2$, and the monolayer-water interfacial area in the highest-curvature region of a stalk is $\sim 50\ nm^2$. For example, it is conceivable that several fusion peptides could bind to the monolayers of the fusion patch before stalk formation, or stabilize the interfaces of a nascent stalk. Another possible energy-reducing arrangement may be disposition of positive charges on the surfaces of proteins immediately surrounding the fusion patch. If arrayed in a semitoroidal geometry around the fusion patch, these might interact with negatively charged lipids on the surface monolayer of a nascent stalk, effectively stabilizing the negative curvature of this surface. For catenoidal fusion pores, most of the Gaussian and mean curvature is concentrated in the region within several nanometers of the minimum radius of the pore (19). Protein binding to the lipid-water interface in this region could lower the curvature energy of the nascent catenoidal fusion pore.

Recently, a fusogenic peptide derived from the fusion-mediating protein of the HIV virus was reported to reduce the k_m of PC membranes by a factor of 3 or more relative to the pure lipid at peptide/lipid molar ratios of only 0.01–0.03, which corresponds to the concentrations expected at fusion sites in vivo (91). The modulus was measured by analyzing the wavelike fluctuations of bilayers in an L_α phase. As noted by Tristram-Nagle and Nagle (91), it is possible that the apparent reduction in k_m is due to a special arrangement of peptides in the bilayers, so that the reduction might not be the same for deformations such as those found in stalk formation. Ideally, the effect of the peptide on the monolayer bending modulus should be measured via osmotic stress experiments in the H_{II} phase (32), where the curvature of the interface is more similar to the curvature expected in a stalk. However, the data in Tristram-Nagle and Nagle (91) show that fusion-mediating peptides can create a lipid-peptide assembly with drastically different elastic constants than the initial lipid monolayer. In a recent theoretical study, Zemel et al. (92) showed that amphiphilic helical peptides that adsorb to the lipid-water interface strongly reduce the bilayer thickness, but also induce either strong positive or negative bilayer curvature, depending on the depth of insertion of the helix. Peptide binding can also simultaneously increase in bilayer bending elastic modulus by as much as severalfold. Both of these effects occurred at a peptide/lipid ratio of only 0.05. The induced bilayer spontaneous curvature ranged between -0.3 and $+\ 0.1\ nm^{-1}$. Only rigid cylindrical peptides were treated in Zemel et al. (92), and the peptide effects on the Gaussian modulus were not calculated. Rigid cylinders that interact strongly with the hydrophobic monolayer interior would probably increase the energy necessary to make membrane or monolayer deformations with nonzero K (92). However, this may not be true of anisotropic inclusions like bent or kinked amphipathic helices bound to lipid-water interfaces, which could stabilize a monolayer in a configuration with $K < 0$ (93,94), effectively lowering the local value of κ.

How would a large peptide-binding-induced change in k_m, alone, affect the curvature energies of stalks forming from the same patch of opposed membranes? In Eq. 19, F_s^0 is the splay elastic energy of a stalk when $J_s = 0$, whose value depends on the value of k_m and the elastic constant for gradients in molecular tilt along lipid interfaces, for which there is no directly determined value (2). No analytical expression for F_s^0 in terms of k_m and tilt elastic constants was given in the studies by Kozlovsky and co-workers (2,11). If peptide binding to the membranes reduces k_m as profoundly as the fusion

peptide in Tristram-Nagle and Nagle (91), it is likely that the value of F_s^0 would be decreased. For low-curvature lipid systems like DOPC, this could reduce the stalk curvature energy. However, because $J_s < 0$, Eq. 19 is the sum of the negative term in $k_m J_s$ and two large and positive contributions, from F_s^0 and from the term in κ. For the low-J_s systems, DOPE and equimolar DOPC/cholesterol, if peptides profoundly decrease the value of k_m, the reduction in absolute magnitude in the $k_m J_s$ term could offset or exceed the effect on F_s^0. Thus, the effect of a change in k_m is sensitive to the local value of J_s.

In contrast, even small peptide-induced changes in κ alone would have large effects on the curvature energies of stalks and catenoidal fusion pores of all lipid compositions. The Gaussian curvature elastic contribution to the total curvature energy is large and positive for stalks and catenoidal fusion pores in all three lipid compositions (Table 2). Increasing κ by 20% (i.e., making it less negative) lowers the total stalk and catenoidal fusion pore energies by ~20 and 40 k_BT, respectively (Table 2). The fusion intermediate energy is especially sensitive to changes in κ, in both low- and high-curvature lipid systems.

However, it is more realistic to consider the effects of peptide-induced changes in combinations of elastic constants. It is unlikely that binding of peptides to the lipid-water interface can change any of the elastic moduli of the lipid monolayers independently of the others. k_m, J_s, and κ are all related to the monolayer stress profile, which is the horizontal force as a function of depth in the plane of the monolayer (15). The first moment of the stress profile along the direction perpendicular to the monolayer is equal to $-k_m J_s$, and the second moment to κ (15). Binding peptides to the monolayer-water interface will change the distribution of mass and intermolecular forces as a function of depth, which should have at least some effect on both moments of the stress profile, and hence on all three quantities. Moreover, peptide adsorption to the monolayer can change the bilayer thickness (95) and, hence, δ. The curvature energies of the fusion intermediates are sensitive to relative changes in different elastic constants. The expression for the curvature energy of stalks (Eq. 19) can be rearranged to yield

$$F_s = F_s^0 + 26.1\,[k_m \delta J_s - 0.452\kappa]. \quad (22)$$

The term in brackets in Eq. 22 is almost identical to the term in brackets in the expression for F_{pore} (Eq. 20). Thus, we see that the curvature energies of stalks and of catenoidal fusion pores in symmetric bilayers are both linearly dependent on nearly the same quantity. To determine the effect of a change in lipid-peptide monolayer composition of the fusion patch on fusion intermediate energy, we generally must determine the change that is produced in the quantity $(k_m \delta J_s - \kappa/2)$. For catenoidal fusion pores in asymmetric bilayers like biomembranes, the bending energy component of F_{pore} is more complicated than in Eq. 20, and will depend on the values of k_m, J_s, and δ for each monolayer, as well as on the catenoidal pore radius. However, the Gaussian curvature elastic contribution to F_{pore} will be proportional to the sum of the κ values for the two monolayers (Eq. 8). Thus, the expression for F_{pore} in the asymmetric bilayer case will have a form similar to Eq. 20 in the sense that F_{pore} will be proportional to the difference between two terms: an expression in terms of bending energy constants, and the sum of Gaussian curvature elastic moduli for the two monolayers.

The two terms inside the brackets in Eqs. 20 and 22 are of similar absolute magnitude, so small simultaneous changes in more than one constant can lead to large changes in total fusion intermediate energy, including large reductions. For example, if peptide-lipid interactions induce a simultaneous 25% increase in κ and 25% decrease in $k_m \delta J_s$ in a patch of equimolar DOPC/cholesterol, then the stalk energy decreases by ~50 k_BT relative to the peptide-free monolayer. This would be partially offset by an increase in F_s^0, and it is presumed that this increase can be no more than 25% (assuming a direct proportionality of F_s^0 to k_m), or ~20 k_BT. The net reduction in stalk energy of >30 k_BT is comparable to the activation energy reductions required for fusion protein activity that were estimated above.

The degree to which isolated peptides change the energy of stalks and catenoidal fusion pores can be inferred from the effects of the peptides on the stability of the R and Q_{II} phases. The free energy of the stalk-based rhombohedral phase (60) is linearly dependent on $(k_m \delta J_s - 0.452\kappa)$ (11). The quantity $(k_m \delta J_s - \kappa/2)$ is the stability criterion for Q_{II} phase to the second order in curvature; Q_{II} phases are stable when this quantity is <0 (18). In a sense, preparing samples of these two phases is like preparing large samples of lipidic fusion intermediates in the laboratory. Insight into which elastic constants are most affected by binding of isolated peptides can be obtained by measuring the peptide effects on J_s, k_m, and δ. J_s and k_m can be determined in the presence of peptide by appropriate x-ray diffraction experiments on peptide-lipid-alkane H_{II} phases (32), and δ by x-ray diffraction experiments on peptide-lipid L_α phases. Such studies make the assumption that the peptides are not maintained in some particular orientation to the bilayers by the structure of the other proteins around the fusion site in vivo, however. Some care must be taken in interpreting the results from R phases. So far, R phases have only been observed (60) at low water activities (0.4–0.8), and lipid elastic constants may be different under such dry conditions from those in excess water (11).

The effects of bilayer-spanning peptides may be especially interesting to study more extensively. Peptides corresponding to the bilayer-spanning regions of viral (96,97) and SNARE (98) fusion proteins, as well as synthetic bilayer-spanning peptides (99), accelerate fusion in otherwise protein-free lipid vesicles (96–99). At least some synthetic membrane-spanning peptides have also been shown to lower the temperature at which Q_{II} phases form by as much as 20° at peptide/lipid ratios of 0.005 (100). It can be shown that this

corresponds to a reduction of 20 k_BT in catenoidal pore energy compared to the pure lipid. It is not clear how the peptides affect the free energy of the Q_{II} phase (100): if the peptides change one or more monolayer elastic constants, the peptides are at such a low concentration that an individual peptide must somehow be able to influence the elastic behavior on the length scale comparable to the interpeptide separation of >8 nm. If such is the case, particular species of membrane-spanning peptides at the periphery of the fusion patch could also reduce the stalk curvature energy.

The author is grateful to M. M. Kozlov for useful discussions.

REFERENCES

1. Markin, V. S., and J. P. Albanesi. 2002. Membrane fusion: stalk mechanism revisited. *Biophys. J.* 82:693–712.
2. Kozlovsky, Y., and M. M. Kozlov. 2002. Stalk model of membrane fusion: solution of energy crisis. *Biophys. J.* 82:882–895.
3. Kozlovsky, Y., L. V. Chernomordik, and M. M. Kozlov. 2002. Lipid intermediates in membrane fusion: formation, structure, and decay of the hemifusion diaphragm. *Biophys. J.* 83:2634–2651.
4. May, S. 2002. Structure and energy of fusion stalks: the role of membrane edges. *Biophys. J.* 83:2969–2980.
5. Siegel, D. P. 2005. Lipid membrane fusion. *In* The Structure of Biological Membranes, 2nd ed. P. L. Yeagle, editor. CRC Press, Boca Raton, FL. 243–308.
6. Chernomordik, L. V., and M. M. Kozlov. 2003. Protein-lipid interplay in fusion and fission of biological membranes. *Annu. Rev. Biochem.* 72:175–207.
7. Chernomordik, L. V., and M. M. Kozlov. 2008. Mechanics of membrane fusion. *Nat. Struct. Mol. Biol.* 15:675–683.
8. Chernomordik, L. V., and M. M. Kozlov. 2005. Membrane hemifusion: crossing a chasm in two leaps. *Cell.* 123:375–382.
9. Chernomordik, L. V., J. Zimmerberg, and M. M. Kozlov. 2006. Membranes of the world unite! *J. Cell Biol.* 175:201–207.
10. Leikin, S. L., M. M. Kozlov, L. V. Chernomordik, V. S. Markin, and Y. A. Chizmadzhev. 1987. Membrane fusion: overcoming of the hydration barrier and local restructuring. *J. Theor. Biol.* 129:411–425.
11. Kozlovsky, Y., A. Efrat, D. P. Siegel, and M. M. Kozlov. 2004. Stalk phase formation: effects of dehydration and saddle splay modulus. *Biophys. J.* 87:2508–2521.
12. Siegel, D. P. 1993. Energetics of intermediates in membrane fusion: comparison of stalk and inverted micellar intermediate mechanisms. *Biophys. J.* 85:2124–2140.
13. Helfrich,W. 1973. Elastic properties of lipid bilayers: theory and possible experiments. *Z. Naturforsch. C.* 28:693–703.
14. Siegel, D. P. 1999. The modified stalk mechanism of lamellar-to-inverted phase transitions and its implications for membrane fusion. *Biophys. J.* 76:291–313.
15. Seddon, J. 1990. Structure of the inverted hexagonal (H_{II}) phase, and non-lamellar phase transitions of lipids. *Biochim. Biophys. Acta.* 1031:1–69.
16. Shearman, G. C., O. Ces, R. H. Templer, and J. M. Seddon. 2006. Inverse lyotropic phases of lipids and membrane curvature. *J. Phys. Condens. Matter.* 18:S1105–S1124.
17. Templer, R. H., B. J. Khoo, and J. M. Seddon. 1998. Gaussian curvature modulus of an amphiphile monolayer. *Langmuir.* 14:7427–7434.
18. Siegel, D. P., and M. M. Kozlov. 2004. The Gaussian curvature elastic modulus of *N*-monomethylated dioleoylphosphatidylethanolamine: relevance to membrane fusion and lipid phase behavior. *Biophys. J.* 67:366–374.
19. Siegel, D. P. 2006. Determining the ratio of the Gaussian curvature and bending elastic moduli of phospholipids from Q_{II} phase unit cell dimensions. *Biophys. J.* 91:608–618.
20. Cherezov, V., D. P. Siegel, W. Shaw, S. W. Burgess, and M. C. Caffrey. 2003. The kinetics of non-lamellar phase formation in DOPE-Me: relevance to membrane fusion. *J. Membr. Biol.* 195:165–182.
21. Lee, J. K., and B. R. Lentz. 1997. Evolution of lipidic structures during model membrane fusion and the relation of this process to cell membrane fusion. *Biochemistry.* 36:6251–6259.
22. Kasson, P. M., N. W. Kelley, N. Singhal, M. Vrljic, A. T. Brunger, and V. S. Pande. 2003. Ensemble molecular dynamics yields submillisecond kinetics and intermediates of membrane fusion. *Proc. Natl. Acad. Sci. USA.* 103:11916–11921.
23. Chanturiya, A., L. V. Chernomordik, and J. Zimmerberg. 1997. Flickering fusion pores comparable with initial exocytotic pores occur in protein-free phospholipid bilayers. *Proc. Natl. Acad. Sci. USA.* 94:14423–14428.
24. Siegel, D. P., W. J. Green, and Y. Talmon. 1994. The mechanism of lamellar-to-inverted hexagonal phase transitions: a study using temperature-jump cryo-electron microscopy. *Biophys. J.* 66:402–414.
25. Kuzmin, P. I., J. Zimmerberg, Y. A. Chizmadzhev, and F. S. Cohen. 2001. A quantitative model for membrane fusion based on low-energy intermediates. *Proc. Natl. Acad. Sci. USA.* 98:7235–7240.
26. Hamm, M. and M. M. Kozlov. 2000. Elastic energy of tilt and bending of fluid membranes. *Eur. Phys. J. E.* 3:323–335.
27. May, S., Y. Kozlovsky, A. Ben-Shaul, and M. M. Kozlov. 2004. Tilt modulus of a lipid monolayer. *Eur. Phys. J. E.* 14:299–308.
28. Siegel, D. P., and B. Tenchov. 2008. Influence of the lamellar phase unbinding energy on the relative stability of lamellar and inverted cubic phases. *Biophys. J.* 94:3987–3995.
29. Marsh, D. 2006. Elastic curvature constants of lipid monolayers and bilayers. *Chem. Phys. Lipids.* 144:146–159.
30. Rand, R. P., and V. A. Parsegian. 1989. Hydration forces between phospholipid bilayers. *Biochim. Biophys. Acta.* 988:351–376.
31. Nagle, J. F., and S. Tristram-Nagle. 2000. Structure of lipid bilayers. *Biochim. Biophys. Acta.* 1469:159–195.
32. Rand, R. P., N. L. Fuller, S. M. Gruner, and V. A. Parsegian. 1990. Membrane curvature, lipid segregation, and structural transitions for phospholipids under dual-solvent stress. *Biochemistry.* 29:76–87.
33. Epand, R. M., N. Fuller, and R. P. Rand. 1996. Role of the position of unsaturation on the phase behavior and intrinsic curvature of phosphatidylethanolamines. *Biophys. J.* 71:1806–1810.
34. Kozlov, M. M., and W. Helfrich. 1992. Effects of a cosurfactant on the stretching and bending elasticities of a surfactant monolayer. *Langmuir.* 8:2792–2797.
35. Keller, S. L., S. M. Bezrukov, S. M. Gruner, M. W. Tate, I. Vodyanov, and V. A. Parsegian. 1993. Probability of alamethicin conductance states varies with nonlamellar tendency of bilayer phospholipids. *Biophys. J.* 65:23–27.
36. Leikin, S., M. M. Kozlov, N. L. Fuller, and R. P. Rand. 1996. Measured effects of diacylglycerol on structural and elastic properties of phospholipid membranes. *Biophys. J.* 71:2623–2632.
37. Chen, Z., and R. P. Rand. 1997. The influence of cholesterol on phospholipid membrane curvature and bending elasticity. *Biophys. J.* 73:267–276.
38. Szule, J. A., N. L. Fuller, and R. P. Rand. 2002. The effects of acyl chain length and saturation of diacylglycerols and phosphatidylcholine on membrane monolayer curvature. *Biophys. J.* 83:977–984.
39. Fuller, N. L., and R. P. Rand. 2001. The influence of lysolipids on the spontaneous curvature and bending elasticity of phospholipid membranes. *Biophys. J.* 81:243–254.
40. Gruner, S. M., M. W. Tate, G. L. Kirk, P. T. C. So, D. C. Turner, D. T. Keane, C. P. S. Tilcock, and P. R. Cullis. 1988. X-Ray-diffraction

study of the polymorphic behavior of N-methylated dioleoylphosphatidylethanolamine. *Biochemistry*. 27:2853–2866.

41. Tate, M. W., and S. M. Gruner. 1989. Temperature eependence of the structural dimensions of the inverted hexagonal (H_{II}) phase of phosphatidylethanolamine-containing membranes. *Biochemistry*. 28: 4245–4253.
42. Shyamsunder, E., S. M. Gruner, M. W. Tate, D. C. Turner, P. T. C. So, and C. P. S. Tilcock. 1988. Observation of inverted cubic phase in hydrated dioleoylphosphatidylethanolamine membranes. *Biochemistry*. 27:2332–2336.
43. Erbes, J., C. Czeslik, W. Hahn, R. Winter, M. Rappolt, and G. Rapp. 1994. On the existence of bicontinuous cubic phases in dioleoylphosphatidylethanolamine. *Ber. Bunsenges. Phys. Chem.* 98:1287–1293.
44. Veiro, J. A., R. G. Khalifah, and E. S. Rowe. 1990. P-31 nuclear nagnetic resonance studies of the appearance of an isotropic component in dielaidoylphosphatidylethanolamine. *Biophys. J.* 57:637–641.
45. Tenchov, B., R. Koynova, and G. Rapp. 1998. Accelerated formation of cubic phases in phosphatidylethanolamine dispersions. *Biophys. J.* 75:853–866.
46. Toombes, G. E. S., A. C. Finnefrock, M. W. Tate, and S. M. Gruner. 2002. Determination of the L_{α}-H_{II} phase transition temperature for 1,2 dioleoyl-*sn*-glycero-3-phosphatidylethanolamine. *Biophys. J.* 82:2504–2510.
47. Hamm, M., and M. M. Kozlov. 1998. Tilt model of inverted amphiphilic mesophases. *Eur. Phys. J. B*. 6:519–528.
48. Chen, Z., and R. P. Rand. 1998. Comparative study of the effects of several *n*-alkanes on phospholipid hexagonal phases. *Biophys. J.* 74:944–952.
49. Ellens, H., D. P. Siegel, D. Alford, P. L. Yeagle, L. Boni, L. J. Lis, P. J. Quinn, and J. Bentz. 1989. Membrane fusion and inverted phases. *Biochemistry*. 28:3692–3703.
50. Tilcock, C. P. S., P. R. Cullis, and S. M. Gruner. 1986. On the validity of P-31-NMR determinations of polymorphic phase behavior. *Chem. Phys. Lipids*. 40:47–56.
51. Gagné, J., L. Stamatatos, T. S. Diacovo, W. Hui, P. L. Yeagle, and J. R. Silvius. 1985. Physical properties and surface interactions of bilayer membranes containing N-methylated phosphatidylethanolamines. *Biochemistry*. 24:4400–4408.
52. Siegel, D. P., J. Banschbach, D. Alford, H. Ellens, L. J. Lis, P. J. Quinn, P. L. Yeagle, and J. Bentz. 1989b. Physiological levels of diacylglycerols in phospholipid membranes induce membrane fusion and stabilize inverted phases. *Biochemistry*. 28:3703–3709.
53. Yeagle, P. L., R. M. Epand, C. D. Richardson, and T. D. Flanagan. 1991. Effects of the ''fusion peptide'' from measles virus on the structure of N-methyl dioleoylphosphatidylethanolamine membranes and their fusion with Sendai virus. *Biochim. Biophys. Acta*. 1065: 49–53.
54. van Gorkum, L. C. M., S. Q. Nie, and R. M. Epand. 1992. Hydrophobic lipid additives affect membrane stability and phase behavior of N-monomethyldioleoylphosphatidyl-ethanolamine. *Biochemistry*. 31:671–677.
55. Epand, R. M., and R. F. Epand. 1994. Relationship between the infectivity of influenza virus and the ability of its fusion peptide to perturb bilayers. *Biochem. Biophys. Res. Commun.* 202:1420–1425.
56. Davies, S. M. A., R. F. Epand, J. P. Bradshaw, and R. M. Epand. 1998. Modulation of lipid polymorphism by the feline leukemia virus fusion peptide: implications for the fusion mechanism. *Biochemistry*. 37:5720–5729.
57. Tilcock, C. P. S., M. B. Bally, S. B. Farren, and P. R. Cullis. 1982. Influence of cholesterol on the structural preferences of dioleoylphosphatidylethanolamine dioleoylphosphatidylcholine systems: a P-31 and deuterium nuclear magnetic resonance study. *Biochemistry*. 21:4596–4601.
58. Tenchov, B. G., R. C. MacDonald, and D. P. Siegel. 2006. Cubic phases in phosphatidylcholine-cholesterol mixtures: cholesterol as membrane ''fusogen''. *Biophys. J.* 91:2508–2516.
59. Kozlov, M. M., and L. V. Chernomnordik. 1998. A mechanism of protein-mediated fusion: coupling between refolding of the influenza hemagglutinin and lipid rearrangements. *Biophys. J.* 75:1384–1396.
60. Yang, L., L. Ding, and H. W. Huang. 2003. New phases of phospholipids and implications to the membrane fusion problem. *Biochemistry*. 42:6631–6635.
61. Efrat, A., L. V. Chernomordik, and M. M. Lozlov. 2007. Point-like protrusions as a prestalk intermediate in membrane fusion pathway. *Biophys. J.* 92:L61–L63.
62. Weaver, J. C., and R. A. Mintzer. 1981. Decreased bilayer stability due to transmembrane potentials. *Phys. Lett.* 86A:57–59.
63. Siegel, D. P., and R. M. Epand. 1997. The mechanism of lamellar-to-inverted hexagonal phase transitions in phosphatidylethanolamine: implications for membrane fusion mechanisms. *Biophys. J.* 73:3088–3111.
64. Reference deleted in proof.
65. Tate, M. W., E. Shyamsunder, S. M. Gruner, and K. L. D'Amico. 1992. Kinetics of the lamellar-inverse hexagonal phase transition determined by time-resolved x-ray diffraction. *Biochemistry*. 31:1081–1092.
66. Malinin, V. S., P. Frederik, and B. R. Lentz. 2002. Osmotic and curvature stress affect PEG-induced fusion of lipid vesicles but not mixing of their lipids. *Biophys. J.* 82:2090–2100.
67. Yang, Q., Y. Guo, L. Li, and S. W. Hui. 1997. Effects of lipid headgroup and packing stress on poly(ethylene glycol)-induced phospholipid vesicle aggregation and fusion. *Biophys. J.* 73:277–282.
68. Kozlov, M. M., and M. Winterhalter. 1991. Elastic moduli and neutral surface for strongly curved monolayers. Analysis of experimental results. *Journal de Physique II*. 1:1085–1100.
69. Kozlov, M. M., S. Leikin, and R. P. Rand. 1994. Bending, hydration and interstitial energies quantitatively account for the hexagonal-lamellar-hexagonal reentrant phase transition in dioleoylphosphatidylethanolamine. *Biophys. J.* 67:1603–1611.
70. Zhang, J., A. Pekosz, and R. A. Lamb. 2000. Influenza virus assembly and lipid raft microdomains: a role for the cytoplasmic tails of the spike glycoproteins. *J. Virol.* 74:4634–4644.
71. Blough, H. A. 1971. Fatty acid composition of individual phospholipids of influenza virus. *J. Gen. Virol.* 12:317–320.
72. Rothman, J. E., D. K. Tsai, E. A. Dawidowicz, and J. Lenard. 1976. Transbilayer phospholipid asymmetry and its maintenance in the membrane of influenza virus. *Biochemistry*. 15:2361–2370.
73. Kawasaki, K., and S. C. Ohnishi. 1992. Membrane fusion of influenza virus with phosphatidylcholine liposomes containing viral receptors. *Biochem. Biophys. Res. Commun.* 186:378–384.
74. Stegmann, T. 1993. Influenza hemagluttinin-mediated membrane fusion does not involve inverted phase lipid intermediates. *J. Biol. Chem.* 268:1716–1722.
75. Alford, D., H. Ellens, and J. Bentz. 1994. Fusion of influenza virus with sialic acid-bearing target membranes. *Biochemistry*. 33:1977–1987.
76. Shangguan, T., D. Alford, and J. Bentz. 1996. Influenza virus-liposome lipid mixing is leaky and largely insensitive to the material properties of the target membrane. *Biochemistry*. 35:4956–4965.
77. Deutsch, J. W., and R. B. Kelly. 1981. Lipids of synaptic vesicles: relevance to the mechanism of membrane fusion. *Biochemistry*. 20:378–385.
78. Takamori, S., M. Holt, K. Stenius, E. A. Lemke, M. Grønborg, D. Riedel, H. Urlaub, S. Schenk, B. Brügger, P. Ringler, S. A. Müller, B. Rammner, F. Gräter, J. S. Hub, B. L. de Groot, G. Mieskes, Y. Moriyama, J. Klingauf, H. Grubmüller, J. Heuser, F. Wieland, and R. Jahn. 2006. Molecular anatomy of a trafficking organelle. *Cell*. 127:831–846.
79. Michaelson, D. M., G. Barkai, and Y. Barenholz. 1983. Asymmetry of lipid organization in cholinergic synaptic vesicle membranes. *Biochem. J.* 211:155–162.

80. Wadel, K., E. Neher, and T. Sakaba. 2007. The coupling between synaptic vesicles and Ca^{2+} channels determines fast neurotransmitter release. *Neuron.* 53:563–575.

81. Wölfel, M., X. Lou, and R. Schneggenburger. 2007. A mechanism intrinsic to the vesicle fusion machinery determines fast and slow transmitter release at a large CNS synapse. *J. Neurosci.* 27:3198–3210.

82. Churchward, M. A., T. Rogasevskaia, D. M. Brandman, H. Khosravani, P. Nava, J. K. Atkinson, and J. R. Coorssen. 2008. Specific lipids supply critical negative spontaneous curvature: an essential component of native Ca^{2+}-triggered membrane fusion. *Biophys. J.* 94:3976–3986.

83. Churchward, M. A., T. Rogasevskaia, J. Hofgen, J. Bau, and J. R. Coorssen. 2005. Cholesterol facilitates the native mechanism of Ca^{2+}-trigered membrane fusion. *J. Cell Sci.* 118:4833–4848.

84. Churchward, A., D. M. Brabdman, T. Rogasevskaia, and J. R. Coorssen. 2008. Copper (II) sulfate charring for high sensitivity on-plate fluorescent detection of lipids and sterols: quantitative analyses of the composition of functional secretory vesicles. *J. Chem. Biol.* DOI 10.1007/s12154-008-0007-1.

85. Zimmerberg, J., C. Sardet, and D. Epel. 1985. Exocytosis of sea urchin egg cortical vesicles in vitro is retarded by hyperosmotic sucrose: kinetics of fusion monitored by quantitative light-scattering microscopy. *J. Cell Biol.* 101:2398–2410.

86. Biswas, S., S.-R. Yin, P. S. Blank, and J. Zimmerberg. 2008. Cholesterol promotes hemifusion and pore widening in membrane fusion induced by influenza hemagglutinin. *J. Gen. Physiol.* 131:503–513.

87. Farsad, K., and P. de Camilli. 2003. Mechanisms of membrane deformation. *Curr. Opin. Cell Biol.* 15:372–381.

88. Zimmerberg, J., and M. M. Kozlov. 2006. How proteins produce cellular membrane curvature. *Nat. Rev. Mol. Cell Biol.* 7:9–19.

89. Martens, S., and H. T. McMahon. 2008. Mechanisms of membrane fusion: disparate players and common principles. *Nat. Rev. Mol. Cell Biol.* 9:543–556.

90. Martens, S., M. M. Kozlov, and H. T. McMahon. 2007. How synaptotagmin promotes membrane fusion. *Science.* 316:1205–1208.

91. Tristram-Nagle, S., and J. F. Nagle. 2007. HIV-1 fusion peptide decreases the bending energy and promotes curved fusion intermediates. *Biophys. J.* 93:1–8.

92. Zemel, A., A. Ben-Shaul, and S. May. 2008. Modulation of the spontaneous curvature and bending rigidity of lipid membranes by interfacially adsorbed amphiphilic peptides. *J. Phys. Chem. B.* 112:6988–6996.

93. Fournier, J. B. 1996. Nontopological saddle-splay and curvature instabilities from anisotropic membrane inclusions. *Phys. Rev. Lett.* 76:4436–4439.

94. Kralj-Iglič, V., V. Heinrich, S. Svetina, and B. Žekš. 1999. Free energy of closed membrane with anisotropic inclusions. *Eur. Phys. J. B.* 10:5–8.

95. Chen, F. Y., M. T. Lee, and H. W. Huang. 2003. Evidence for membrane thinning effect as the mechanisms fro peptide-induced pore formation. *Biophys. J.* 84:3751–3758.

96. Langosch, D., B. Brosig, and R. Pipkorn. 2001. Peptide mimetics of the vesicular stomatitis virus G-protein transmembrane segment drive membrane fusion in vitro. *J. Biol. Chem.* 276:32016–32021.

97. Dennison, S. M., N. Greenfield, J. Lenard, and B. R. Lentz. 2002. VSV transmembrane domain (TMD) peptide promotes PEG-mediated fusion of liposomes in a conformationally sensitive fashion. *Biochemistry.* 41:14925–14934.

98. Langosch, D., J. M. Crane, B. Brosig, A. Hellwig, L. K. Tamm, and J. Reed. 2001. Peptide mimetics of SNARE transmembrane segments drive membrane fusion depending on their conformational plasticity. *J. Mol. Biol.* 311:709–721.

99. Hofman, M. W., K. Weise, J. Ollesch, P. Agrawal, H. Stalz, W. Stelzer, F. Hulsbergen, H. de Groot, K. Gerwert, J. Reed, and D. Langosch. 2004. De novo design of conformationally flexible transmembrane peptides driving membrane fusion. *Proc. Natl. Acad. Sci. USA.* 101:14776–14781.

100. Siegel, D. P., V. Cherezov, D. V. Greathouse, R. E. Koeppe II, J. A. Killian, and M. C. Cafferty. 2006. Transmembrane peptides stabilize inverted cubic phases in a biphasic length-dependent manner: implications for protein-induced membrane fusion. *Biophys. J.* 90:200–211.